

# Non-linear Dynamics and Primordial Black Hole Formation During Kination

Cheng Cheng,<sup>1,\*</sup> Panagiotis Giannadakis,<sup>1,†</sup> Lucien Heurtier,<sup>1,‡</sup> and Eugene A. Lim<sup>1,§</sup>

<sup>1</sup>*Theoretical Particle Physics and Cosmology Group, Physics Department,  
King's College London, Strand, London WC2R 2LS, United Kingdom*

We investigate the effects of large scalar inhomogeneities during the kination epoch, a period in which the universe's dynamics are dominated by the kinetic energy of a scalar field, by fully evolving the Einstein equations using numerical relativity. By tracking the non-linear growth of scalar perturbations with both sub-horizon and super-horizon initial wavelengths, we are able to compare their evolution to perturbative results. Our key findings show that in the deep sub-horizon limit, the perturbative behaviour remains valid, whereas in the super-horizon regime, non-linear dynamics exhibit a much richer phenomenology. Finally, we discuss the possibility of primordial black hole formation from the collapse of such perturbations and assess whether this process could serve as a viable mechanism to reheat the universe in the post-inflationary era.

## I. INTRODUCTION

The standard cosmological narrative begins with a period of slow-roll inflation [1–3], during which the dynamics are governed by a scalar field—the inflaton—rolling down a nearly flat potential. This phase provides solutions to the horizon and flatness problems, while also stretching quantum fluctuations of the inflaton field, which later seeds the formation of large-scale structures. After inflation ends, it is usually assumed that the inflationary sector reheats the universe by transferring most of its energy to Standard Model particles. This marks the beginning of the Hot Big Bang phase, initially characterized by a radiation-dominated plasma with an equation-of-state parameter  $w = 1/3$ , which eventually transitions to matter domination with  $w = 0$ , as the universe cools. Interestingly, there are no strong constraints on the equation of state of the universe during the period between the end of inflation and the onset of reheating. This opens up the possibility for a variety of cosmological scenarios. One such possibility is that the post-inflationary—but pre-reheating—epoch is a phase during which the universe's dynamics are dominated by the kinetic energy of a rolling scalar field, which may be the inflaton or another scalar. This phase, referred to as *kination*, was first proposed in [4], characterised by equation-of-state parameter  $w = 1$ . For a more comprehensive review of kination we refer the reader to [5]. Kination is especially relevant in the context of string theory, where ultra-light moduli fields can dominate early-universe dynamics [6]. String cosmology models involving either the inflaton or other moduli may naturally give rise to kination if the relevant modulus potential features a steep region at the end of inflation—where the potential decreases exponentially,

enabling the field to acquire significant kinetic energy—followed by a flat region where the field eventually slows down. What happens afterward depends on the exact shape of the potential.

Suppose the potential is of a runaway form, the field slows down via Hubble friction, possibly initiating a secondary period of slow-roll inflation. It is worth noting that this feature is common in *quintessential* inflation models [7–12] and more generally, in non-oscillatory inflation scenarios [13, 14], where the inflaton field undergoes (i) a slow-roll phase in the early universe, (ii) a phase of acceleration as the potential decreases sharply and the universe enters into a kination era, and (iii) a second phase of slow-roll during which the field decelerates to eventually either behave like a cosmological constant or track the universe's background energy density at late times [13–17]. On the other hand, if the potential features a local minimum, the field may eventually settle into it, acquiring a finite mass and oscillating before decaying to reheat the universe, as occurs in the so-called Large Volume Scenarios (LVS) [17–19].

The existence of a long kination era within the cosmological timeline may leave imprints in cosmological data that could be searched for in the foreseeable future [20–22]. However, the authors of [17, 23, 24] pointed out that, according to perturbation theory, such a kination era is expected to be unstable due to the growth of scalar-field perturbations. Unlike the homogeneous background field, these perturbations behave like a relativistic perfect fluid with an equation-of-state parameter of  $w = 1/3$ . The authors of [24] showed that such scalar perturbations may act as a background for the homogeneous scalar field, which ends up tracking its own perturbation and eventually behaves like radiation. Generally speaking, such considerations suggest that a kination era may not exceed  $\sim 10 - 11$   $e$ -folds [17, 23]. In [17, 23, 24], the fate of small scalar perturbations is explored in the context of an initially kinetic-energy-dominated background where the gravitational backreaction is ignored. Perturbation

\* [cheng.2.cheng@kcl.ac.uk](mailto:cheng.2.cheng@kcl.ac.uk)

† [panagiotis.giannadakis@kcl.ac.uk](mailto:panagiotis.giannadakis@kcl.ac.uk)

‡ [lucien.heurtier@kcl.ac.uk](mailto:lucien.heurtier@kcl.ac.uk)

§ [eugene.a.lim@gmail.com](mailto:eugene.a.lim@gmail.com)

theory has provided valuable insights into this regime; however, its main limitation is that it cannot capture strong gravitational effects or backreaction.

In this work, we are instead interested in the evolution of kination in the presence of non-linear perturbations where strong gravitational effects and backreaction can play an important role. This becomes particularly important during kination, where even initially small scalar field perturbations—especially those of large super-horizon wavelength—can be significantly amplified. As these modes re-enter the Hubble horizon, they may dominate the local dynamics, inducing sharp *local* gradient inhomogeneities that strongly backreact on the background geometry. Consequently, the study of perturbations during kination transitions into a strong-gravity problem. In scenarios where the backreaction becomes sufficiently strong, gravitational collapse may occur, potentially leading to black hole formation. In this context, while perturbation theory provides essential guidance, this regime necessitates the use of tools from numerical relativity.

We find that for sub-horizon perturbations, even for relatively large initial amplitudes, gravitational backreaction remains weak and does not induce collapse. In this case, scalar perturbations *on average* evolve like radiation for scales much larger than the perturbation scales, in agreement with perturbative predictions. Gravitational backreaction only becomes significant with initial perturbation energy density much larger than the kination background energy density. In this scenario, the notion of a kination background is no longer clear. On the other hand, for linear super-horizon perturbations, gravitational collapse becomes significantly more likely after horizon re-entry. We provide a quantitative analysis of the critical initial overdensity required for collapse and compare it with perturbative expectations. Our results indicate that black hole formation is generally easier during kination than in perturbative analysis. This has important implications for the shape and amplitude of the power spectrum necessary to produce a significant primordial black hole abundance in the early universe.

This paper is organised as follows: In Section II we provide an introductory framework on kination and our numerical simulation setups, in Section III we present our numerical results for sub-horizon and super-horizon perturbations respectively, focusing on the conditions for black hole formation in the super-horizon case. In Section IV we discuss cosmological implications for the production of primordial black holes in cosmology, and we conclude in Section V. In this work, we use the non-reduced Planck mass,  $m_P^2 \equiv \hbar c/G = G^{-1}$  with  $\hbar = c = 1$  for theoretical analysis, and we use geometric units with  $G = c = 1$  for simulation works.

## II. THEORY AND METHODOLOGY

### A. Perturbations in Kination Epoch

In order to study the dynamics during the kination epoch, we consider a single scalar field minimally coupled to gravity with a potential  $V(\phi)$  which, in a post-inflationary scenario, is expected to feature a long (trans-Planckian) region where the potential is decaying exponentially such as in LVS models or quintessence. In such potential configurations, the scalar field can roll for an extended period, acquiring large canonical momentum while the potential remains subdominant, namely  $V(\phi) \ll \frac{1}{2}\dot{\phi}^2$ . The relevant action is given by:

$$S = \int d^4x \sqrt{-g} \left( \frac{m_P^2}{16\pi} R - \frac{1}{2}(\nabla\phi)^2 - V(\phi) \right), \quad (1)$$

where  $R$  denote the Ricci scalar.

For simplicity, we restrict ourselves to the case where the dynamics are dominated by the kinetic energy of the homogeneous scalar field, allowing us to work in the limit where  $V(\phi) \rightarrow 0$ . In this regime, the equation of motion is given by

$$\ddot{\phi} + 3H\dot{\phi} - \nabla^2\phi = 0. \quad (2)$$

$$H^2 \equiv \left( \frac{\dot{a}}{a} \right)^2 = \frac{8\pi}{3m_P^2} \left( \frac{1}{2}\dot{\phi}^2 + \frac{1}{2}(\nabla\phi)^2 \right). \quad (3)$$

Before fully solving Einstein's equations and investigating the effect of non-linear dynamics on the system, let us briefly recap basic results from cosmological perturbation theory, in which the full field solution  $\phi(t, x) \equiv \bar{\phi}(t) + \delta\phi(t, \vec{x})$  is decomposed into a homogeneous background solution and small spatial perturbations. The background energy density consists purely of kinetic energy, such that

$$\bar{\rho} \equiv \frac{1}{2}\dot{\phi}^2 \propto a^{-6}. \quad (4)$$

Meanwhile, the linear perturbations behave as  $\rho_{\delta\phi} \propto a^{-4}$  in the sub-horizon regime,  $k \gg H$ , and  $\rho_{\delta\phi} \propto a^{-2}$  in the super-horizon regime,  $k \ll H$ . For more details on perturbation theory, we refer the reader to Appendix A.

In the homogeneous limit where  $\delta\phi = 0$ ,  $\rho \equiv \bar{\rho} \propto a^{-6}$ , until another fluid with a different equation-of-state parameter starts dominating. However, in the presence of perturbations, the situation becomes more interesting because the energy density of the background field redshifts faster than the energy density of its own perturbations. Whenever a notion of a homogeneous background field can be defined—as is the case in the presence of Gaussian and deeply sub-horizon perturbations—the metric evolution is still well described by standard FLRW cosmology. This could lead to the domination of the perturbations, and possibly to tracker solutions in the presence of a subdominant potential, as shown in [24].

However, for perturbations with sizes comparable to or larger than the Hubble horizon, such perturbations might grow sufficiently for strong gravity effects to become significant at horizon scales. In this case, the FLRW metric may no longer be an accurate description of the space-time: such configurations could either lead to a space-time dominated by radiation-like perturbations or, alternatively, strong backreaction on the geometry might lead to gravitational collapse and black hole formation.

Depending on the abundance and amplitude of super-horizon perturbations, the formation of such primordial black holes (PBHs) may play an important role in cosmology, as it could lead to a period of early matter domination after kination with observational consequences. The critical value of the overdensity associated with a curvature perturbation at the time it enters the horizon,  $\delta_c$ , is essential to the calculation of such a PBH abundance (see e.g. [25, 26]). The value of this critical overdensity was studied analytically using a *three-zone* solution (a spherically symmetric top-hat overdensity surrounded by a matching region, itself embedded in an FLRW universe) by [27] and has the following form

$$\delta_c = \frac{3(1+w)}{5+3w} \sin^2 \left( \frac{\pi\sqrt{w}}{1+3w} \right), \quad (5)$$

which, for pure kination, corresponds to  $w = 1$  and  $\delta_c = 0.375$ . One of the primary goals of what follows is to test the robustness of this analytical result using numerical relativity.

## B. Initial Scalar Data

Our simulation domain is a 3-dimensional box with length  $L$  and periodic boundary conditions. We adopt a “pseudo-isotropic” setup, with a sinusoidal inhomogeneity of the scalar field in all three spatial directions, while keeping the kinetic background homogeneous:

$$\phi_0 = \bar{\phi}_0 + \frac{\Delta\phi}{3} \sum_{i=1}^3 \cos \left( \frac{2\pi N_{\phi,0} x_i}{L} \right), \quad (6)$$

$$\dot{\phi}_0 = \sqrt{\frac{3}{4\pi}} m_P H_0 \quad (7)$$

where the subscript “0” denotes a quantity evaluated at initial time,  $x_i$  labels the spatial coordinates on the hyperslice evolving by the time coordinate  $t$ ,  $\bar{\phi}_0$  is the initial homogeneous scalar field,  $\Delta\phi$  is the amplitude of the sinusoidal inhomogeneities,  $N_{\phi,0}$  is the mode number of the initial scalar field inhomogeneity,  $H_0$  is the initial Hubble parameter in the absence of the inhomogeneity, i.e. in pure kination limit. In this work, we have chosen to study the fate of a single self-perturbation mode of a scalar field. A thorough treatment of a full spectrum of modes and the effects of kinetic inhomogeneity is beyond the scope of this paper and is left for future investigation.

Since  $V \ll \frac{1}{2}\dot{\phi}^2$  during a kination era, we consider the simple case where  $V(\phi) = 0^1$ . Therefore, the dynamics are insensitive to translations in field space, and we are allowed to choose the initial background field value to be  $\bar{\phi}_0 = 0$ . Since we impose periodic boundary conditions, the size of the simulation domain,  $L$ , is chosen to be the initial scalar field inhomogeneity wavelength, which is proportional to the initial Hubble length

$$L \equiv (N_{\phi,0} H_0)^{-1} = (N_{\phi,0} \dot{\phi}_0)^{-1} \sqrt{\frac{3}{4\pi}} m_P. \quad (8)$$

With this setup, the gradient energy density, defined as

$$\rho_{\nabla} \equiv \frac{1}{2} \gamma^{ij} \partial_i \phi \partial_j \phi. \quad (9)$$

will be the sole contributor to the initial perturbation energy density. We can compute its average at initial time to be

$$\langle \rho_{\nabla,0} \rangle = \frac{\Delta\phi^2 N_{\phi,0}^2 \pi^2}{3L^2}, \quad (10)$$

where  $\langle \rangle$  denotes the volume average over the spatial hyperslice, defined as

$$\langle X \rangle \equiv \frac{\int_{\Sigma} d^3x \sqrt{\gamma} X}{\int_{\Sigma} d^3x \sqrt{\gamma}}. \quad (11)$$

We introduce the *non-linearity* parameter

$$b \equiv \frac{\langle \rho_{\nabla,0} \rangle}{\bar{\rho}_0}, \quad (12)$$

with

$$\bar{\rho}_0 \equiv \frac{1}{2} \dot{\phi}_0^2 \quad (13)$$

which indicates the non-linearity of the initial inhomogeneity and allows us to tune the amplitude of the scalar field inhomogeneity accordingly.

## C. Initial Geometric Data

We foliate our spacetime following the ADM formulation with the metric

$$ds^2 = -\alpha^2 dt^2 + \gamma_{ij} (dx^i + \beta^i dt)(dx^j + \beta^j dt), \quad (14)$$

where the quantities  $\alpha$  and  $\beta^i$  are the lapse and shift functions that are evolving as gauge choices encoding the coordinate freedom of general relativity, while  $\gamma_{ij}$  is the 3-dimensional spatial metric of the spatial hyperslice. The

<sup>1</sup> Note that for this reason, we would not observe in our work the tracker solution described in [24] due to the absence of a potential.

spatial metric and the gauge quantities are evolving along with the extrinsic curvature  $K_{ij} = \partial_t \gamma_{ij} + D_{(i} \beta_{j)}$ , with  $D_i$  the 3-dimensional covariant derivative with respect to  $\gamma_{ij}$ , which acts as the canonical momentum of the metric in the Hamiltonian formulation of General Relativity.

The extrinsic curvature is then further decomposed into its trace and traceless part:

$$K_{ij} = A_{ij} + \frac{1}{3} \gamma_{ij} K, \quad (15)$$

where the trace part  $K$  is associated with the local expansion or contractions of spacetime. The traceless term  $A_{ij}$  can be further decomposed into transverse and longitudinal components where the former is the usual “gravitational wave” degrees of freedom in the linear limit. The spatial metric can be also be decomposed as  $\gamma_{ij} = \chi^{-1} \tilde{\gamma}_{ij}$  with  $\chi$  being the conformal factor such that  $\det(\tilde{\gamma}) = 1$ .

We impose periodic boundary conditions, which means that we set the initial size of the simulation domain to a characteristic scale and the universe consists of infinitely many such boxes. In the limit of FLRW spacetimes, the Hubble length grows as  $H^{-1} \sim a^3$  during kination; while the wavelength of a single mode stretches proportionally to  $a$ . Therefore, while the mode is stationary in the simulation domain, its characteristic wavelength is decreasing relative to the Hubble length due to the size of the domain shrinking compared to the physical Hubble volume.

Given an initial scalar field configuration, the initial data for the hyperslice is solved with the CTTK method [28, 29], where we assume an initially conformally flat with spatial metric  $\tilde{\gamma}_{ij} = \delta_{ij}$ . For the initial hyperslice we assume  $\alpha_0 = 1$ ,  $\beta_0^i = B_0^i = 0$ , and fix the conformal factor  $\chi = 1$  everywhere. This leads to an algebraic equation for the Hamiltonian constraint and a Poisson-like equation for the momentum constraint, which are solved to obtain the initial profiles of the local expansion parameter  $K$  and trace-free extrinsic curvature  $A_{ij}$ .

Additionally, the use of periodic boundary conditions enforces integrability conditions on the constraint equations. Specifically, the integral of the constraints over the simulation domain must vanish. Setting  $\chi = 1$  implies that  $\int d^3x \Pi \partial_i \phi = 0$ , at the initial slice.

#### D. Evolution and Diagnostics

We evolve the system of the geometric and matter quantities with the CCZ4 [30] evolution scheme, see details in the [31, 32].

In the FLRW limit, the Hamiltonian constraint equation is identified with the Friedmann equation, where Hubble parameter is the trace of the extrinsic curvature  $H = -\frac{1}{3}K$ . Throughout this work except for explicit mentioning, we are using a coarse-grained measure of the expansion, the volume-averaged conformal factor:

$$a = \langle \chi \rangle^{-1/2}, \quad (16)$$

which naturally translates to the scale factor in FLRW limit.

For the evolution of the gauge quantities, we choose a modified version of moving puncture gauge [33, 34] where the lapse is evolving as:

$$\partial_t \alpha = -2\alpha(K - \langle K \rangle - 2\Theta) + \beta^i \partial_i \alpha, \quad (17)$$

This gauge choice maintains the lapse function roughly at its initial value for relatively homogeneous expanding regions while approaching the 1+log form in collapsing regions with  $\langle K \rangle < 0$ . It thus better regularises the behaviour of the lapse function in a cosmological spacetime. We adopt the standard Gamma-driver condition

$$\partial_t \beta^i = \frac{3}{4} B^i, \quad (18)$$

$$\partial_t B^i = \partial_t \tilde{\Gamma}^i - B^i. \quad (19)$$

In this work, we focus on studying the evolution of the scalar field in the presence of a self-perturbation. Inhomogeneities in the form of gradient energy induce gravitational backreaction and result in kinetic inhomogeneities. This also contribute to the perturbation energy density. To study how the total perturbation energy density behaves, we need to identify both the gradient and kinetic perturbation energy densities.

In numerical relativity, we use the gauge parameters to define the conjugate momentum of the scalar field as

$$\Pi \equiv \frac{1}{\alpha} (\dot{\phi} - \beta^i \partial_i \phi_0). \quad (20)$$

This allows us to define the volume-averaged perturbation energy density as

$$\langle \rho_{\delta\phi} \rangle \equiv \langle \rho_{\nabla} \rangle + \langle \rho_K \rangle - \langle \bar{\rho} \rangle, \quad (21)$$

with

$$\langle \rho_K \rangle \equiv \frac{1}{2} \langle \Pi^2 \rangle, \quad (22)$$

$$\langle \bar{\rho} \rangle \equiv \frac{1}{2} \langle \Pi \rangle^2. \quad (23)$$

This practically means the perturbation energy density is equal to the average gradient density plus the variance of the kinetic energy.

The growth of perturbation with respect to the kination background, explained above could eventually lead to a significant local overdensity. Such local overdensity could reach above a critical point and lead to the formation of a black hole. The formation and presence of a black hole is tracked by calculating if an apparent horizon has formed in the hyperslice [35].

We calculate the masses of the black holes by measuring the minimum area of the apparent horizon. As there

is no initial angular momentum in the system, we can approximate the black hole mass with the Schwarzschild radius,  $M_{\text{BH}}^2 \approx r_{\text{BH}}^2/4 \approx A_{\text{AH}}/16\pi$ . In geometric units,  $[M] \sim [L] \sim [T]$ . We will denote the Hubble scale at the start of the kination period as  $H_{\text{kin},0}$ . We define our geometric mass according to [36]

$$H_{\text{kin},0} = H_0 \left( \frac{Mg}{m_P} \right)^n, \quad (24)$$

with  $H_0 = 1/(N_{\phi,0}L)$  defined in Eq. (8), and  $n = -1$  denotes the dimensionality of  $H$  in geometric units. The masses of the black holes in Planck units are then converted in a similar fashion with

$$M_{\text{BH,pl}} = M_{\text{BH,g}} \left( \frac{Mg}{m_P} \right). \quad (25)$$

### III. NUMERICAL RESULTS

For our simulations, we use the multi-purpose numerical relativity code `GRChombo` [31, 37]. We tune the initial inhomogeneity amplitude and the field momentum based on the ratio  $b$  defined in Eq. (12). Our goal is to investigate the fate of the spacetimes when large scalar inhomogeneities emerge in a kination background. We present our results based on the initial characteristic wavelengths of the inhomogeneities. Perturbations with  $\lambda_0 < H_0^{-1}$  constitute initially sub-horizon inhomogeneities and conversely,  $\lambda_0 > H_0^{-1}$ , super-horizon inhomogeneities.

#### A. Sub-Horizon and Near-Horizon Scale Perturbations

In this section, we investigate the effects of both large and small amplitude inhomogeneities in the sub-horizon regime, where  $\lambda < H_0^{-1}$ . In the perturbation theory limit, sub-horizon modes evolve as  $\rho_{\delta\phi} \sim a^{-4}$ , indicating a behaviour that resembles radiation. According to [23], this behaviour is robust regardless of whether the inhomogeneities are in the linear or non-linear regime in the presence of a fixed background. We aim to investigate the behaviour of the scalar self-perturbation in a pure kination regime, allowing the inhomogeneities to evolve into the non-linear regime and potentially become the dominant energy density contribution. As stated above, one normally expects the presence of a subdominant potential term, which may nevertheless remain subdominant in the post-inflationary evolution compared to the kinetic energy density and can therefore be safely neglected.

We simulate a scalar field with an initially homogeneous kinetic energy profile, superimposed with an inhomogeneity characterized by an initial wavelength of  $\lambda = 0.01H_0^{-1}$  as in Eq. (6). The amplitude of this inhomogeneity is chosen such that the volume-averaged initial gradient energy density is a tenth of the kinetic energy density, i.e.

$b = 0.1$ . To focus on the localised dynamics, we capture only a single full wavelength of the perturbation within our simulation domain instead of the entire Hubble volume. We study the evolution of this perturbation by tracking the volume-averaged perturbation energy density defined in Eq. (21). We present our results in Figure 1.

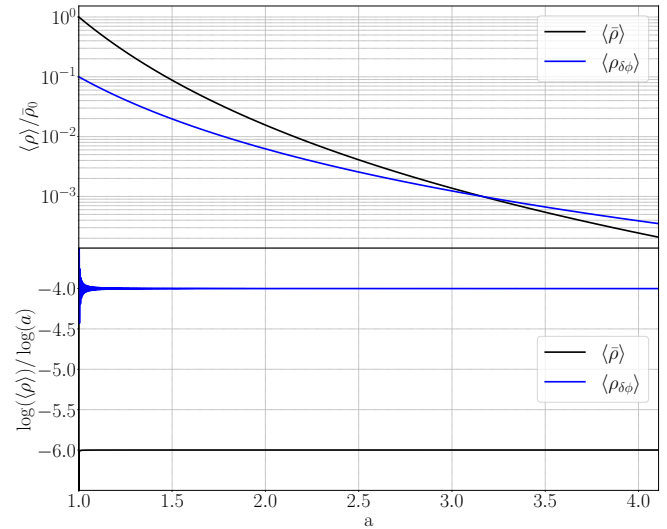


FIG. 1. Simulation results for  $\lambda_0 = 0.01H_0^{-1}$ ,  $b = 0.1$  – at  $a \sim 3$ , the “perturbation” energy  $\rho_{\delta\phi}$  dominates over the “background” energy density, but the two “components” still evolve as  $a^{-4}$  and  $a^{-6}$  respectively. **Upper panel:** the evolution of volume-averaged energy densities of the background and perturbation. **Lower panel:** background and perturbation energy densities as a power law of the volume-averaged scale factor  $a = \langle \chi \rangle^{-1/2}$ .

We found that a sub-horizon mode in the subdominant regime indeed behaves as  $\langle \rho_{\delta\phi} \rangle \sim a^{-4}$ . It redshifts as  $a^{-4}$ , becomes  $\mathcal{O}(1)$  with the kination background, and dominates as an effective radiation-like background. The continuity in the energy density profiles in Figure 1 shows that the transition from kination domination to radiation domination is smooth.

As [38, 39] has shown that direct collapse black hole formation is possible with a supercritical sub-horizon initial overdensity during matter domination, we investigate such processes for kination. We discovered that for inhomogeneities with characteristic wavelengths of  $\lambda \sim \mathcal{O}(10^{-1})H_0^{-1}$  the critical overdensity is of  $\mathcal{O}(10^2 \sim 10^3)$ . In such conditions, the universe’s evolution is dominated by a highly localised gradient energy density of a massless scalar field. Therefore, gravitational collapse via accretion is highly suppressed. We thus conclude that, even if sub-horizon perturbations manage to grow during a kination era to become  $\mathcal{O}(1)$ , it is still very unlikely for such perturbations to undergo gravitational collapse.

As we probe sub-horizon inhomogeneities with wavelengths closer to the horizon size, the critical value  $b_{\text{crit}}$

for black hole formation is reduced. For  $\lambda_0 = 0.5H_0^{-1}$ , we find  $b_{\text{crit}} \approx 20$ , which still implies that gradients must initially be very dominant. Once black holes form in our simulation, the universe becomes matter-dominated, with black holes forming on a lattice due to the symmetries enforced by the periodic boundary conditions.

In the near-Hubble limit, where  $\lambda_0 = H_0^{-1}$ , we find that black hole formation can occur more easily, with a critical value  $b_{\text{crit}} \approx 2$ . We note that while the wavelength is nominally of Hubble size, the significant amount of energy density from the gradient of the scalar field effectively shrinks the actual Hubble sphere, rendering the inhomogeneity effectively super-horizon. In the limit of such large inhomogeneities at this length scale, it is not meaningful to associate the energy density evolution with the scale factor, nor is the scale factor itself well-defined due to the lack of homogeneity. In cases where black holes do not form, we observe that the energy density eventually, on average, evolves as in a radiation-dominated universe. Additionally, for near-Hubble wavelengths, with  $b \ll 1$ , the perturbations grow relative to the kination background and eventually dominate the evolution, again behaving like a radiation-dominated universe in the same manner as in the deep sub-horizon case.

To conclude this section: in the limit where a kination background with small perturbations is present, the perturbation theory result remains valid—namely, small perturbations redshift more slowly than the kinetic background and eventually dominate the dynamics of the universe, becoming a new “background” that behaves like radiation, with the kinetic background becoming subdominant. On the other hand, when the initial  $b \gtrsim 1$ , inhomogeneities dominate the evolution, but the gravitational backreaction is not strong enough to induce large-scale collapse. However, we checked that in the limit  $b \gg 1$ , gravitational collapse can occur although this is not a surprise: sufficiently large homogeneities will always dominate local dynamics and cause collapse.

## B. Super-Horizon Perturbations

For inhomogeneities with characteristic wavelength  $\lambda_0 > H_0^{-1}$ , perturbation theory predicts that the perturbation energy density of super-horizon modes is approximately given by the gradient term and scales as  $\rho_{\delta\phi} \sim \rho_{\nabla} \sim a^{-2}$ . Thus, it effectively “grows” as  $a^4$  compared to the kination background and behaves like scalar curvature perturbations. However, in practice, as shown in the previous section that the energy density of the perturbations consists of both the gradient term and the induced kinetic term. Thus, we aim to investigate whether the perturbation energy density and/or the gradient energy density still behave as  $\rho_{\delta\phi} \sim a^{-2}$  in the presence of induced kinetic inhomogeneity and strong gravitational backreaction.

We begin by confirming this in the linear limit and sim-

ulate a scalar field with a homogeneous kinetic energy profile and an inhomogeneity characterised by an initial wavelength of  $\lambda_0 = 10^4 H_0^{-1}$ . The amplitude of this inhomogeneity is chosen by setting the non-linearity parameter to  $b = 10^{-10}$ . The results of the simulation are shown in Figure 2. We find that once the system relaxes from the initial conditions, the volume-averaged perturbation energy density closely tracks the gradient energy density. We measure the variance of the local expansion parameter  $\langle \delta K \rangle / \langle K \rangle \ll 1$ , indicating that the simulation domain remains highly homogeneous and the spacetime closely follows the FLRW metric. We are thus justified in identifying  $\langle \chi \rangle^{-1/2} \sim a$  and the perturbation energy density does evolve as  $\langle \rho_{\delta\phi} \rangle \sim \langle \rho_{\nabla} \rangle \sim a^{-2}$  in this linear regime.

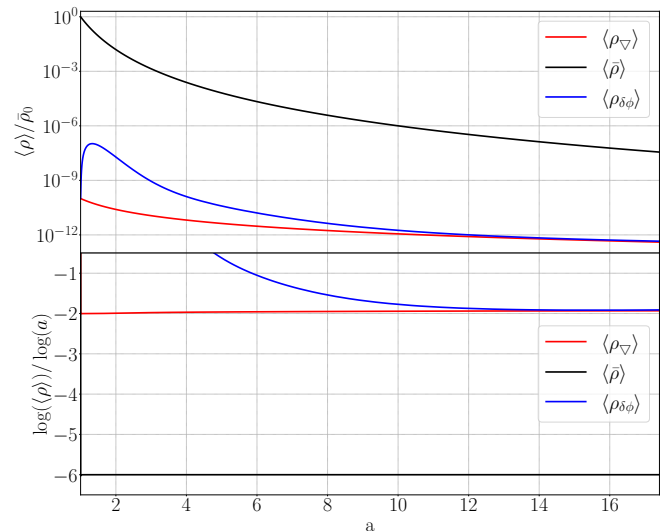


FIG. 2. Simulation results for  $\lambda_0 = 10^4 H_0^{-1}$ ,  $b = 10^{-10}$ . The perturbation energy density is closely tracked by the gradient energy density and evolve as  $\langle \rho_{\delta\phi} \rangle \sim \langle \rho_{\nabla} \rangle \sim a^{-2}$  while the kination background remains at  $\langle \bar{\rho} \rangle \sim a^{-6}$ . **Upper panel:** the evolution of volume-averaged energy densities of the background, the gradient, and perturbations, **Lower panel:** background, gradient, and perturbation energy densities as a power law of the volume-averaged scale factor  $a = \langle \chi \rangle^{-1/2}$ .

We extend the simulation duration to investigate whether these perturbations continue to behave as  $\langle \rho_{\delta\phi} \rangle \sim a^{-2}$  when they enter a non-linear regime. Since the oscillation period of the super-horizon mode is proportional to the characteristic wavelength,  $T \propto \lambda \gg H^{-1}$ , for the mode to oscillate and eventually re-enter the horizon to potentially enter a strong-gravity regime, we shorten the initial characteristic wavelength and increase the initial gradient energy density. We present a representative case with  $\lambda_0 = 200H_0^{-1}$  and  $b = 1.8 \times 10^{-6}$  in Figure 3.

We observe that while the perturbation energy density is initially “attracted” to  $\langle \rho_{\delta\phi} \rangle \sim a^{-2}$  initially as perturbation theory suggests, the behaviours of both  $\langle \rho_{\delta\phi} \rangle$  and  $\langle \rho_{\nabla} \rangle$  quickly deviate from a constant power law once the

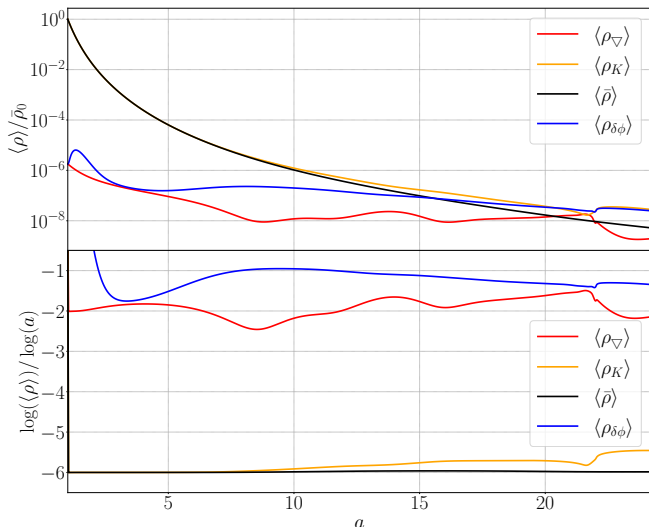


FIG. 3. Simulation results for  $\lambda_0 = 200H_0^{-1}$ ,  $b = 1.8 \times 10^{-6}$ . The formation of black hole is indicated by the discontinuity around  $a_{\text{BH}} \sim 22$  at the end of the plot. The perturbation energy density deviates away from the perturbative description and shifts towards  $\langle \rho_{\delta\phi} \rangle \sim a^{-1}$ , with the gradient energy density fluctuates around  $\langle \rho_{\nabla} \rangle \sim a^{-2}$ . **Upper panel:** the evolution of volume-averaged energy densities of the background, gradient, kinetic, and perturbations, **Lower panel:** The background, gradient, kinetic, and perturbation energy densities as a power law of the volume-averaged conformal factor  $\langle \chi \rangle^{-1/2}$ . Simulation movie: <https://youtu.be/rPnIBkoagwM>

oscillatory behaviour of the super-horizon mode and the induced kinetic perturbation energy density becomes significant. In particular, the behaviour for the total perturbation evolves approximately as  $\langle \rho_{\delta\phi} \rangle \sim a^{-1}$ , while the gradient term exhibits an oscillatory behaviour around  $\langle \rho_{\nabla} \rangle \sim a^{-2}$ . This indicates that the oscillatory behaviour and strong gravitational backreaction are significant.

Since during kination, the Hubble length redshifts as  $H^{-1} \sim a^3$ , while the wavelength of the mode redshifts as  $\lambda \sim a$ , we can approximate the horizon re-entry at

$$a_{\text{re-entry}} \approx \sqrt{\lambda_0 H_0}. \quad (26)$$

This estimate assumes a consistent and well-defined notion of the scale factor throughout the simulation domain and evolution. To ensure this, we verify that the domain remains well-described by an FLRW spacetime. Following the methods of [36, 40] we evaluate the variance,  $\sigma^2$ , of the local expansion parameter. In scenarios where black hole formation is expected, we additionally monitor the variance of the conformal factor and compute their kurtoses,  $g_2^2$ , to assess deviation from FLRW

behaviour near the onset of gravitational collapse. In the simulation shown in Figure 3, we observe that both  $\sigma_K^2$  and  $\sigma_\chi^2$  remain in the range  $\mathcal{O}(10^{-3} \sim 10^{-5})$  throughout the evolution. We also find that  $g_{2,\chi} \sim g_{2,K} \sim -1$  prior to the black hole formation showing platykurtic (or near uniformity) distribution. These results confirm that the spacetime remains an excellent approximation to FLRW before the onset of black hole formation.

In the example shown in Figure 3, we estimate the horizon re-entry to occur at  $a_{\text{re-entry}} \approx 14$  with  $\langle \rho_{\delta\phi} \rangle \lesssim \langle \bar{\rho} \rangle$  and black hole formation at  $a_{\text{BH}} \approx 22$  as indicated by the discontinuity in the energy density profiles. The first detection of an apparent horizon and the estimated mode horizon re-entry are separated by approximately 0.5  $e$ -folds. We observed that this behaviour is consistent across all super-horizon modes we have tested.

As mentioned above, we aim to investigate whether the critical overdensity is robust for super-horizon modes that exhibit non-linear behaviour before horizon re-entry. We simulated a range of super-horizon modes with initial wavelengths spanning from  $5H_0^{-1}$  to  $2000H_0^{-1}$  and a non-linearity parameter  $b$  ranging from  $\mathcal{O}(10^{-2} \sim 10^{-9})$ . We present the results in Figure 4.

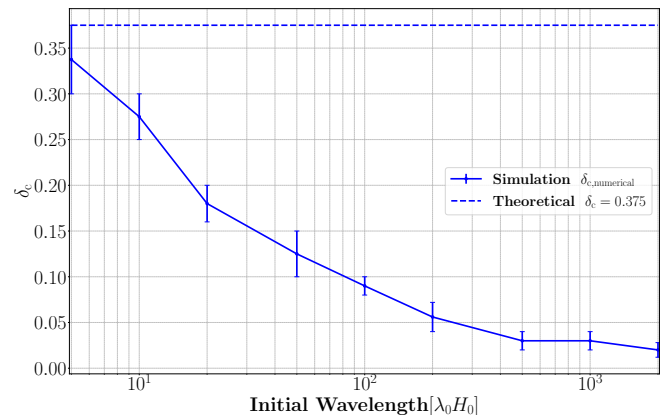


FIG. 4. Extrapolated critical overdensity from numerical simulations for primordial black hole formation compared with the prediction from the Press-Schechter formalism of gravitational collapse [25, 26]. The upper bound of the error bar corresponds the lowest amplitude tested with a black hole formation, whereas the lower bound of the error bar corresponds the highest amplitude tested without a black hole formation, and the solid blue line indicates the central value between the two bounds.

Given the relative growth of the perturbation, the simulation domain deviates from pure FLRW spacetime, making the precise moment of horizon re-entry difficult to

<sup>2</sup> We use the natural estimator definition of

$$g_2 = \frac{\frac{1}{n} \sum_i^n (x_i - \bar{x})^4}{\sigma^4} - 3,$$

where  $\sigma$  is the standard deviation. Under this definition,  $g_2 = -3$  indicates absolute uniformity,  $g_2 = 0$  indicates a normal distribution, and  $g_2 > 0$  indicates a sharp peak in distribution.

define. We define  $\delta_{c, \text{numerical}}$  as the effective critical overdensity, extrapolated from the simulation results under the assumptions that the kinetic energy density always dominates the universe's evolution prior to horizon re-entry, and that the perturbation grows relative to the kination background remains as  $a^4$

$$\delta_{c, \text{numerical}} \approx a^4 b = (\lambda_0 H_0)^2 b \quad (27)$$

Therefore the presented values do not represent the critical overdensity for primordial black hole formation at horizon re-entry. Instead, they serve as a comparison to the theoretical predictions if one expects the super-horizon modes to stay frozen as in the perturbative limit, until re-entry, i.e  $\delta \propto a^4$ . Under this assumption, these are the values that correspond to the critical initial conditions that lead to primordial black holes. We detail the cosmological implications in the following section.

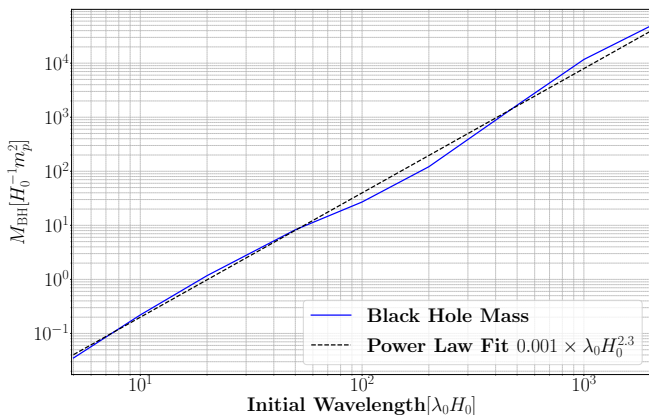


FIG. 5. The mass of the black holes from simulations at the point of formation and a power law fit  $M_{BH} \approx 0.001 \times (\lambda_0 H_0)^{2.3}$

In the simulation where black holes form, the lightest black holes at the point of formation are shown in Figure 5 with respect to the initial Hubble scale. To compare to the Hubble scale at the point of formation, we note that while the volume-averaged perturbation energy density is of  $\mathcal{O}(1)$  compared to the background, the inhomogeneities are concentrated in the proximity of the primordial black hole both before and after formation. Therefore, we are still able to extract the Hubble parameter from the homogeneous bulk region. This corresponds roughly to  $\mathcal{O}(10^{-2} \sim 10^{-3}) H^{-1} m_p^2$ .

The maximum initial wavelength we have tested in this work is  $2000 H_0^{-1}$ . This limitation arises primarily due to the following factors

1. As discussed above, we observe the point of horizon re-entry occurs at  $a_{\text{re-entry}} \approx \sqrt{\lambda_0 H_0}$  with black hole formation typically taking place about  $\sim 0.5$   $e$ -folds later. In this work, the largest scale factor we were able to probe is  $a \sim 80$ . To investigate longer super-horizon modes that would re-enter the

horizon during a prolonged kination era lasting up to  $N_{\text{kin}} \sim 10$ , the simulation would need to reach scale factors of  $\mathcal{O}(10^3 \sim 10^4)$ . However, achieving such large scale factors is currently infeasible with the numerical setup employed in this study. Numerical stability constrains the maximum allowed time step, and reaching significantly larger values of  $a$  leads to an accumulation of numerical errors and requires computational resources that grow exponentially with simulation duration.

2. The gauge choice we have imposed in Eq. (17) ensures that the presence of a small perturbation does not induce strong gravitational backreaction until close to horizon re-entry. Thus the simulation domain is effectively a uniformly expanding spacetime with a decaying expansion rate. In such domains, we observe the local expansion parameter is  $K \lesssim 0$ , with regions fluctuating slightly above and below the average. While Eq. (17) is a more cosmology-friendly gauge [36], the prolonged oscillation periods for longer super-horizon modes gradually drive the lapse value across the entire hyperslice downward. As detailed in II C, the lapse function is initially set to 1 everywhere on the hyperslice. The combined effect of the dynamics and this gauge choice causes the lapse function to drop to  $\mathcal{O}(10^{-1})$  across the domain, thereby increasing both the simulation time and computational cost.

#### IV. IMPLICATIONS FOR COSMOLOGY

Scalar inflation models featuring a runaway direction in field space—and thus naturally leading to a kination era—generically face a challenge: how to reheat a universe dominated by the kinetic energy of a rolling massless scalar field? The most common answer to that question so far was to invoke the gravitational production of SM particles, generating a finite amount of radiation at the end of inflation that eventually overtakes the kination field (see, for instance, [11] and references therein). However, such a gravitational production is typically very inefficient, requiring a prolonged kination phase to be successful<sup>3</sup>

$$N_{\text{kin}} \gtrsim 16.46 + \log \left( \frac{10^{14} \text{GeV}}{H_{\text{end}}} \right), \quad (28)$$

where  $H_{\text{end}}$  denotes the Hubble scale at the end of inflation. From this equation, and given existing upper bounds on the energy scale during inflation [41], one finds that reheating the universe via gravitational reheating

<sup>3</sup> This result is obtained assuming that the SM of particle physics contains  $g_* = 106.75$  relativistic degrees of freedom at the inflation energy scale, and taking the efficiency factor  $q = 1$  in Eq. (26) of [11].

alone after kination requires  $N_{\text{kin}} \gg 10$ . However, such a long period of kination is precisely what was shown recently to be very difficult—if not impossible to sustain—as scalar perturbations appear to dominate over the kination background after about 10  $e$ -folds [5, 24]. This suggests that an alternative mechanism is necessary to reheat the universe following kination.

There exist at least two other plausible mechanisms to reheat the universe after the kination phase ends:

1. The kination field will eventually develop a mass term, allowing it to decay and transfer its energy density to the radiation sector—as exemplified in [17]—or alternatively, a phase transition might abruptly end the kination period, or something else is produced during kination that succeeds in dominating the energy density of the universe above the Big-Bang Nucleosynthesis (BBN) temperature.
2. Primordial Black Holes (PBHs) formed during the kination era could serve this purpose in the second scenario: if produced during kination, they can rapidly dominate the energy density before evaporating and reheating the universe. Indeed, since they constitute a cold matter component of the universe prior to evaporation, PBHs would eventually dominate over both the kination background and the radiation contributions from the scalar perturbations. Whether such PBHs could reheat the universe thus depends on their initial abundance and lifetime, such that they evaporate only after they have begun dominating.

Let us henceforth assume that the primordial power spectrum of scalar curvature perturbations  $\Delta_{\mathcal{R}}^2(k)$  features—beyond the nearly scale-invariant contribution  $\Delta_{\mathcal{R},\text{CMB}}^2$  responsible for the CMB modes—a quasi-monochromatic enhancement at a specific wave-number  $k_{\text{PBH}}$ , such that

$$\Delta_{\mathcal{R}}^2(k) = \Delta_{\mathcal{R},\text{CMB}}^2(k) + \Delta_{\mathcal{R},\text{peak}}^2 \delta(k - k_{\text{PBH}}). \quad (29)$$

Typically, the power spectrum responsible for the perturbations observed in the CMB has an amplitude too small to produce any primordial black holes (PBHs), resulting in fewer than one PBH per Hubble patch. However, in the presence of features along the inflation trajectory that lead to brief phases of ultra-slow-roll such as is the case in [25] within the context of kination—the peak amplitude  $\Delta_{\mathcal{R},\text{peak}}^2$  may become large enough to generate a significant fraction of PBHs. This energy fraction of the universe’s energy density at the time of PBH formation, commonly denoted as  $\beta$ , is extremely sensitive to the critical overdensity  $\delta_c$  above which perturbations collapse into black holes at horizon re-entry (see [42]) and scale as

$$\beta \sim \frac{\Delta_{\mathcal{R},\text{peak}}}{\sqrt{2\pi}\delta_c} \exp\left(-\frac{\delta_c^2}{2\Delta_{\mathcal{R},\text{peak}}^2}\right). \quad (30)$$

Demanding that the PBHs form when mode  $k_{\text{PBH}}$  enters the horizon, we find that this fractions needs to

satisfy

$$\beta \gtrsim \left(\frac{\Gamma_{\text{ev}}}{H_{\text{end}}}\right)^{1/2} e^{-\frac{3}{2}N_{\text{kin}} + 3(N_{\text{form}} - N_{\text{end}})}, \quad (31)$$

where we chose  $N_{\text{kin}} \approx 10$  the total number of  $e$ -folds of kination until radiation-like scalar perturbations dominate over the kination background,  $N_{\text{form}} - N_{\text{end}}$  denotes the number of  $e$ -folds between the end of inflation and PBH formation, and  $\Gamma_{\text{ev}} \approx 10^{-2}m_P^4/M^3$  is the evaporation rate of PBHs with mass  $M$ .

In Figure 6, we translate the results obtained in Section III for  $\delta_c$  into lower bounds on  $\Delta_{\mathcal{R},\text{peak}}^2$  that satisfy the condition of Eq. (31) for an arbitrary value of  $H_{\text{end}} = 10^{13}\text{GeV}$ . Nevertheless, due to the logarithmic dependency of  $\Delta_{\mathcal{R},\text{peak}}^2$  on  $\beta$ , we note that the results depend only very mildly on the actual value of  $H_{\text{end}}$ . From the figure, it is clear that the very small values of  $\delta_c$  we obtained for large perturbations (which form at larger  $N_{\text{form}}$ ) reduce the required amplitude of the power spectrum by more than an order of magnitude compared to previous claims in the literature that use the analytical results of [27].

This result is particularly important, as it is generally very challenging—from a model-building perspective—to enhance the power spectrum of comoving scalar curvature perturbations all the way up to  $\Delta_{\mathcal{R},\text{peak}}^2 \sim \mathcal{O}(10^{-2} \sim 10^{-3})$  without requiring significant fine-tuning of the inflaton potential parameters [43]. Moreover, such enhancements often risk conflicting with the CMB predictions, especially regarding the spectral index  $n_s$  and the tensor-to-scalar ratio  $r$ . However, according to our results, the required power spectrum amplitude during a kination era for PBHs to play a significant cosmological role only needs to reach  $\sim \mathcal{O}(10^{-5})$ . Achieving this level of enhancement within an inflationary scenario featuring a transient ultra-slow-roll phase does not suffer from the same fine-tuning issues, and is therefore more plausible from an ultraviolet complete theoretical framework.

## V. SUMMARY AND OUTLOOK

We have studied the evolution of large scalar inhomogeneities during a kination epoch beyond the linear regime using numerical relativity.

Starting with small perturbations, our results in the sub-horizon limit agree with perturbative analysis: linear perturbations grow relative to the background and eventually dominate the universe, but do not collapse into black holes. We then examined initially large perturbations and found that they rapidly begin to behave like radiation unless the initial non-linear parameter is big  $b \gg 1$ , in which case gravitational forces are strong enough to induce immediate collapse into a black hole. However, such large sub-horizon perturbations cannot arise from the growth of initially small fluctuations after horizon

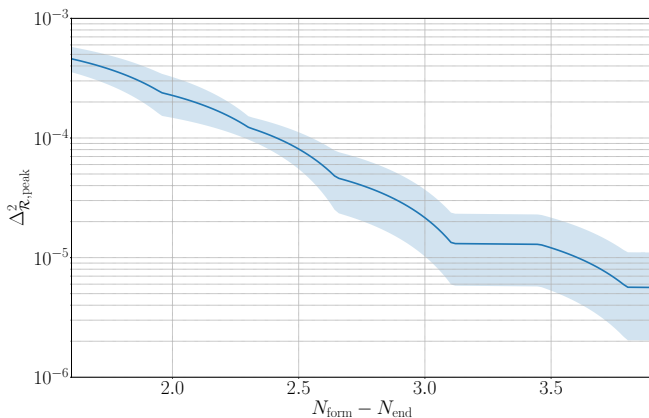


FIG. 6. Minimum peak value of the power spectrum of scalar curvature perturbation necessary to produce enough PBHs,  $N_{\text{form}} - N_{\text{end}}$   $e$ -folds after the end of inflation. The values of  $\delta_c$  used to derive the blue central line and the shaded bands around it correspond to the central values and error bars depicted in Figure 4.

re-entry: their domination over the background would halt further growth, preventing collapse. We therefore conclude that only mechanisms capable of sourcing large sub-horizon inhomogeneities at early times could lead to gravitational collapse.

On the other hand, super-horizon inhomogeneities manifest a much more interesting phenomenology with regard to strong gravity effects. The very long oscillation timescales of these modes imply that they behave like curvature perturbations prior to horizon re-entry. We observed that even in the limit where  $b \ll 1$ , such perturbations grow significantly relative to the background within just a few  $e$ -folds of kination. After horizon re-entry, their fate depends on their amplitude, they may either evolve into a radiation-like background—similar to typical for sub-horizon modes—or collapse into black holes. Our key finding is that the critical overdensity extrapolated from our numerical evolution, is much smaller compared to the perturbative predictions, although it converges to the perturbative predictions when the initial wavelength approaches  $H_0^{-1}$ . For increasingly larger wavelengths, we find that the extrapolated critical overdensity decreases, reaching around  $\delta_{c,\text{numerical}} \approx 0.02$  at  $\lambda_0 \approx 2000H_0^{-1}$ , as shown in Figure 4.

This significant reduction of the extrapolated critical overdensity for the collapse of super-horizon modes into PBHs as compared to previously existing results in the literature is crucial. Indeed, the capacity of Gaussian perturbations—characterized by a primordial power spectrum  $\Delta_{\mathcal{R}}^2$ —to produce PBHs from their horizon re-entry is exponentially sensitive to this critical value,  $\beta \simeq \exp(-\delta_c^2/\Delta_{\mathcal{R}}^2)$ . Reducing  $\delta_c$  by over an order of magnitude thus considerably eases PBH formation. We estimated the typical value that would be required for  $\Delta_{\mathcal{R}}^2$  for PBH formation during kination to lead to PBH

domination and evaporation before BBN, and found that values of  $\mathcal{O}(10^{-5})$  were sufficient—compared to around  $\mathcal{O}(10^{-3})$  in the standard kination scenario.

It is also worth noting that in our numerical simulations, the requirement that the initial spatial hyperslice be conformally flat, combined with the imposition of periodic boundary conditions, enforces a high degree of symmetry in our physical setup. Intuitively, one might expect that in the case of black hole formation, the collapse of a single perturbation mode in three spatial directions might remove some energy from the system to create the spherical configuration that eventually collapses. Therefore, we cannot exclude the scenario in which the numerical value of  $\delta_c$  in the case of direct spherical collapse might be even lower than what we have inferred in section III. It is important that future simulations explore such spherically symmetric configurations so that the expression for  $\delta_c$  can be verified more accurately; in this work, we did not pursue this direction due to the difficulty in finding initial conditions that both respect spherical symmetry and satisfy the integrability conditions imposed by periodic boundary conditions. On the opposite, additional degrees of non-sphericity might as well render the collapse more difficult to achieve [44], which also requires a specific study in the context of kination.

In addition, we have chosen initial conditions corresponding to pure kination, where the scalar potential vanishes and no initial kinetic perturbations are present. While this provides a well-defined setup for studying scalar inhomogeneities, it would be valuable to explore scenarios in which a potential with an exponentially decaying region, as discussed in the Introduction, is included in conjunction with a dynamical geometry. Furthermore, it would be interesting to investigate perturbations in the kinetic sector with varying wavelengths, provided that the integrability conditions remain satisfied.

Finally, it is necessary to comment on the choice of gauge. In our numerical simulations, we employ a modified version of the moving puncture gauge, which includes a contribution from the volume-averaged extrinsic curvature scalar. As explained in Section III, this particular gauge choice leads to the lapse function eventually dropping to very low values, effectively freezing the simulations for very large initial scalar wavelengths. A more suitable gauge could enable the evolution of the system for at least seven  $e$ -folds of kination, potentially allowing for a more accurate determination of  $\delta_c$  in the limit of very large initial wavelengths. We leave such explorations to future work.

## VI. ACKNOWLEDGEMENTS

We acknowledge useful conversations with Martin Mosny, Joseph Conlon, Benjamin Stefanek, and Katy Clough. CC and PG thank Santiago Agüí Salcedo, Gonzalo

Villa, Lucas Vicente Garcia-Consuegra, Josu Calvo Aurrekoetxea, Daniel G. Figueroa and Liina Chung-Jukko for their useful input. We would also like to thank the GR-Chombo team (<http://www.grchombo.org/>). This work is supported by a Research Project Grant RPG-2021-423 from Leverhulme Trust.

This work was performed using the DiRAC@Durham facility managed by the Institute for Computational Cosmology on behalf of the STFC DiRAC HPC Facility ([www.dirac.ac.uk](http://www.dirac.ac.uk)) under DiRAC RAC15 Grant ACTP316. The equipment was funded by BEIS capital funding via STFC capital grants ST/P002293/1,

ST/R002371/1 and ST/S002502/1, Durham University and STFC operations grant ST/R000832/1. This work also used the DiRAC Data Intensive service at Leicester, operated by the University of Leicester IT Services, which forms part of the STFC DiRAC HPC Facility ([www.dirac.ac.uk](http://www.dirac.ac.uk)). The equipment was funded by BEIS capital funding via STFC capital grants ST/K000373/1 and ST/R002363/1 and STFC DiRAC Operations grant ST/R001014/1. DiRAC is part of the National e-Infrastructure. The work of LH is supported by the STFC (grant No. ST/X000753/1).

- 
- [1] A. H. Guth, *Phys. Rev.* **D23**, 347 (1981).  
 [2] A. D. Linde, *Phys. Lett.* **B108**, 389 (1982).  
 [3] A. Albrecht and P. J. Steinhardt, *Phys. Rev. Lett.* **48**, 1220 (1982).  
 [4] M. Joyce, *Physical Review D* **55**, 1875–1878 (1997).  
 [5] Y. Gouttenoire, G. Servant, and P. Simakachorn, “Kination cosmology from scalar fields and gravitational-wave signatures,” (2022), [arXiv:2111.01150](https://arxiv.org/abs/2111.01150) [hep-ph].  
 [6] M. Cicoli, J. P. Conlon, A. Maharana, S. Parameswaran, F. Quevedo, and I. Zavala, “String cosmology: from the early universe to today,” (2023), [arXiv:2303.04819](https://arxiv.org/abs/2303.04819) [hep-th].  
 [7] P. J. E. Peebles and A. Vilenkin, *Phys. Rev. D* **59**, 063505 (1999), [arXiv:astro-ph/9810509](https://arxiv.org/abs/astro-ph/9810509).  
 [8] I. P. Neupane and C. Scherer, *JCAP* **05**, 009 (2008), [arXiv:0712.2468](https://arxiv.org/abs/0712.2468) [astro-ph].  
 [9] J. de Haro and L. Aresté Saló, *Galaxies* **9**, 73 (2021).  
 [10] D. Bettoni and J. Rubio, *Galaxies* **10**, 22 (2022).  
 [11] K. Dimopoulos and C. Owen, *JCAP* **06**, 027 (2017), [arXiv:1703.00305](https://arxiv.org/abs/1703.00305) [gr-qc].  
 [12] K. Dimopoulos and J. W. F. Valle, *Astropart. Phys.* **18**, 287 (2002), [arXiv:astro-ph/0111417](https://arxiv.org/abs/astro-ph/0111417).  
 [13] J. Ellis, D. V. Nanopoulos, K. A. Olive, and S. Verner, *JCAP* **03**, 052 (2021), [arXiv:2008.09099](https://arxiv.org/abs/2008.09099) [hep-ph].  
 [14] L. Heurtier, A. Moursy, and L. Wacquez, *JCAP* **03**, 020 (2023), [arXiv:2207.11502](https://arxiv.org/abs/2207.11502) [hep-th].  
 [15] I. Zlatev, L.-M. Wang, and P. J. Steinhardt, *Phys. Rev. Lett.* **82**, 896 (1999), [arXiv:astro-ph/9807002](https://arxiv.org/abs/astro-ph/9807002).  
 [16] P. J. Steinhardt, L.-M. Wang, and I. Zlatev, *Phys. Rev. D* **59**, 123504 (1999), [arXiv:astro-ph/9812313](https://arxiv.org/abs/astro-ph/9812313).  
 [17] F. Apers, J. P. Conlon, E. J. Copeland, M. Mosny, and F. Revello, “String theory and the first half of the universe,” (2024), [arXiv:2401.04064](https://arxiv.org/abs/2401.04064) [hep-th].  
 [18] V. Balasubramanian, P. Berglund, J. P. Conlon, and F. Quevedo, *Journal of High Energy Physics* **2005**, 007–007 (2005).  
 [19] J. P. Conlon, F. Quevedo, and K. Suruliz, *Journal of High Energy Physics* **2005**, 007–007 (2005).  
 [20] A. Ghoshal, L. Heurtier, and A. Paul, *JHEP* **12**, 105 (2022), [arXiv:2208.01670](https://arxiv.org/abs/2208.01670) [hep-ph].  
 [21] Y. Gouttenoire, G. Servant, and P. Simakachorn, (2021), [arXiv:2111.01150](https://arxiv.org/abs/2111.01150) [hep-ph].  
 [22] A. K. Soman, S. S. Mishra, M. Shafi, and S. Basak, (2024), [arXiv:2407.07956](https://arxiv.org/abs/2407.07956) [gr-qc].  
 [23] C. Eröncel, Y. Gouttenoire, R. Sato, G. Servant, and P. Simakachorn, “A universal bound on the duration of a kination era,” (2025), [arXiv:2501.17226](https://arxiv.org/abs/2501.17226) [hep-ph].  
 [24] M. Mosny, J. P. Conlon, and E. J. Copeland, “Self-tracking solutions for asymptotic scalar fields,” (2025), [arXiv:2507.04161](https://arxiv.org/abs/2507.04161) [hep-th].  
 [25] L. Heurtier, A. Moursy, and L. Wacquez, *Journal of Cosmology and Astroparticle Physics* **2023**, 020 (2023).  
 [26] S. Bhattacharya, S. Mohanty, and P. Parashari, *Physical Review D* **102** (2020), [10.1103/physrevd.102.043522](https://doi.org/10.1103/physrevd.102.043522).  
 [27] T. Harada, C.-M. Yoo, and K. Kohri, *Physical Review D* **88** (2013), [10.1103/physrevd.88.084051](https://doi.org/10.1103/physrevd.88.084051).  
 [28] J. C. Aurrekoetxea, K. Clough, and E. A. Lim, *Class. Quant. Grav.* **40**, 075003 (2023), [arXiv:2207.03125](https://arxiv.org/abs/2207.03125) [gr-qc].  
 [29] J. C. Aurrekoetxea *et al.*, (2025), [arXiv:2501.13046](https://arxiv.org/abs/2501.13046) [gr-qc].  
 [30] M. Dumbser, F. Guercilena, S. Köppel, L. Rezzolla, and O. Zanotti, *Physical Review D* **97** (2018), [10.1103/physrevd.97.084053](https://doi.org/10.1103/physrevd.97.084053).  
 [31] T. Andrade, L. Salo, J. Aurrekoetxea, J. Bamber, K. Clough, R. Croft, E. de Jong, A. Drew, A. Duran, P. Ferreira, P. Figueras, H. Finkel, T. Frana, B.-X. Ge, C. Gu, T. Helfer, J. Jäykkä, C. Joana, M. Kunesch, K. Kornet, E. Lim, F. Muia, Z. Nazari, M. Radia, J. Ripley, P. Shellard, U. Sperhake, D. Traykova, S. Tunyasuvunakool, Z. Wang, J. Widdicombe, and K. Wong, *Journal of Open Source Software* **6**, 3703 (2021).  
 [32] M. Radia, U. Sperhake, A. Drew, K. Clough, P. Figueras, E. A. Lim, J. L. Ripley, J. C. Aurrekoetxea, T. França, and T. Helfer, *Classical and Quantum Gravity* **39**, 135006 (2022).  
 [33] M. Campanelli, C. O. Lousto, P. Marronetti, and Y. Zlochower, *Phys. Rev. Lett.* **96**, 111101 (2006), [arXiv:gr-qc/0511048](https://arxiv.org/abs/gr-qc/0511048) [gr-qc].  
 [34] J. G. Baker, J. Centrella, D.-I. Choi, M. Koppitz, and J. van Meter, *Phys. Rev. Lett.* **96**, 111102 (2006), [arXiv:gr-qc/0511103](https://arxiv.org/abs/gr-qc/0511103) [gr-qc].  
 [35] J. Thornburg, *Classical and Quantum Gravity* **21**, 743–766 (2003).  
 [36] J. C. Aurrekoetxea, K. Clough, and E. A. Lim, *Living Reviews in Relativity* **28** (2025), [10.1007/s41114-025-00058-z](https://doi.org/10.1007/s41114-025-00058-z).  
 [37] K. Clough, P. Figueras, H. Finkel, M. Kunesch, E. A. Lim, and S. Tunyasuvunakool, *Classical and Quantum Gravity* **32**, 245011 (2015).  
 [38] E. de Jong, J. C. Aurrekoetxea, and E. A. Lim, *Journal of Cosmology and Astroparticle Physics* **2022**, 029

- (2022).
- [39] E. de Jong, J. C. Aurrekoetxea, E. A. Lim, and T. França, *JCAP* **10**, 067 (2023), arXiv:2306.11810 [astro-ph.CO].
- [40] J. T. Giblin, J. B. Mertens, and G. D. Starkman, *Physical Review Letters* **116** (2016), 10.1103/physrevlett.116.251301.
- [41] N. Aghanim *et al.* (Planck), *Astron. Astrophys.* **641**, A6 (2020), [Erratum: *Astron. Astrophys.* 652, C4 (2021)], arXiv:1807.06209 [astro-ph.CO].
- [42] C. T. Byrnes and P. S. Cole (2021) arXiv:2112.05716 [astro-ph.CO].
- [43] P. S. Cole, A. D. Gow, C. T. Byrnes, and S. P. Patil, *JCAP* **08**, 031 (2023), arXiv:2304.01997 [astro-ph.CO].
- [44] A. Escrivà and C.-M. Yoo, “Simulations of ellipsoidal primordial black hole formation,” (2024), arXiv:2410.03452 [gr-qc].
- [45] M. Alcubierre, *Introduction to 3+1 Numerical Relativity* (2006), 10.1093/acprof:oso/9780199205677.001.0001.

## Appendix A: Linear Perturbations During Kination

We briefly review the relevant solutions of kination in cosmological perturbation theory context; for a more detailed analysis, we refer the reader to [17, 23, 24]. The scalar field in the presence of small scalar perturbations is expressed as  $\phi \rightarrow \bar{\phi}(t) + \delta\phi(t, \mathbf{x})$  with the perturbation decomposed into Fourier modes as

$$\delta\phi(t, \mathbf{x}) = \int \frac{d^3\mathbf{k}}{(2\pi)^3} \delta\phi_{\mathbf{k}} e^{i\mathbf{k}\cdot\mathbf{x}}. \quad (\text{A1})$$

In Newtonian gauge the metric reads

$$ds^2 = -(1 + 2\Phi)dt^2 + a^2(1 - 2\Phi)\gamma_{ij}dx^i dx^j \quad (\text{A2})$$

In this case the equation of motion for the background scalar field  $\bar{\phi}$  and its perturbation in Fourier space is given by:

$$\ddot{\bar{\phi}} + 3H\dot{\bar{\phi}} = 0, \quad (\text{A3})$$

$$\delta\ddot{\phi}_{\mathbf{k}} + 3H\delta\dot{\phi}_{\mathbf{k}} + \frac{\mathbf{k}^2}{a^2}\delta\phi_{\mathbf{k}} = 4\dot{\Phi}_{\mathbf{k}}\dot{\bar{\phi}}, \quad (\text{A4})$$

with the source term on the right-hand side and the perturbation equation of motion given by the coupling of the Newtonian potential  $\Phi_{\mathbf{k}}$  and the  $\delta\phi_{\mathbf{k}}$  perturbation. The scale factor evolves as

$$a = a_0(t/t_0)^c$$

with  $c = 2/3(1 + w) \equiv 1/3$  for kination and the Hubble parameter  $H = \sqrt{8\pi G/3\bar{\rho}} = c/t$ . To fully obtain the solution in the perturbation theory, the system of those PDEs is closed by the Poisson's equation for the Newtonian potential  $\Phi$

$$\nabla^2\Phi_{\mathbf{k}} = -4\pi G a^2(\rho_{\mathbf{k}} - \bar{\rho}), \quad (\text{A5})$$

where  $\rho_{\mathbf{k}}$  is the Fourier transform of the  $k$  mode energy density. In pure kination with initial conditions  $\bar{\phi}(t_0) = 0$  and  $\dot{\bar{\phi}}(t_0) = \Pi_0$  and the background scalar field evolves as

$$\bar{\phi}(t) = \Pi_0 t_0 \ln\left(\frac{t}{t_0}\right). \quad (\text{A6})$$

If we ignore the source term in the perturbation equation of motion, Eq. A3, the background equation can be solved analytically. In deep sub-horizon limit  $k \gg H_0$  we can obtain an analytical expression with respect to the Bessel functions of zeroth kind:

$$\delta\phi_{\mathbf{k}} = At^{-\frac{3c-1}{2}} J_{\alpha}\left(\frac{ka^{-1}}{1-c}t\right) + Bt^{-\frac{3c-1}{2}} J_{-\alpha}\left(\frac{ka^{-1}}{1-c}t\right) \quad (\text{A7})$$

with

$$\alpha = \frac{3c-1}{2c-2} \equiv 0. \quad (\text{A8})$$

Then from the asymptotic behaviour of zeroth Bessel functions we obtain

$$\delta\phi_{\mathbf{k}} \sim \frac{\cos\left(\frac{ka^{-1}}{1-c}\right)}{a} \sim a^{-1} \quad (\text{A9})$$

We then conclude that the gradient density of the perturbations evolves as

$$\rho_{\text{grad}} \sim \frac{\delta\phi_{\mathbf{k}}^2}{a^2} \sim a^{-4}, \quad (\text{A10})$$

while the kinetic energy of the perturbations

$$\rho_{\text{kin}} \sim \delta\dot{\phi}_{\mathbf{k}}^2 \sim a^{-4}, \quad (\text{A11})$$

and therefore  $\rho_{\delta\phi} \sim a^{-4}$ . In the super-horizon regime  $k \ll H$  and the gradient term can be ignored.

$$\rho_{\delta\phi} \sim \rho_{\text{grad}} \sim \frac{\delta\phi_{\mathbf{k}0}^2}{a^2} \sim a^{-2} \quad (\text{A12})$$

in the limit where the super-horizon modes are frozen. The conclusion is that deep sub-horizon modes grow with respect to the kination background as  $a^4$  while for super-horizon modes as  $a^2$ .

## Appendix B: Convergence Tests

We test the robustness of our numerical simulation by comparing the evolution with initial wavelength  $\lambda_0 = 20H_0^{-1}$  and initial non-linearity parameter  $b = 0.0005$  in three different base resolutions, namely  $N_{LR} = 128$ ,  $N_{MR} = 144$ ,  $N_{HR} = 160$ . Figure 7, we show the volume averaged Hamiltonian constraint violation

$$\mathcal{H} = R^3 + K^2 - K_{ij}K^{ij} - 16\pi\rho \quad (\text{B1})$$

and the differences between the base resolutions, indicating second order convergence prior to the black hole formation according to Eq. (B2).

$$\frac{|\langle\mathcal{H}_{MR}\rangle - \langle\mathcal{H}_{LR}\rangle|}{|\langle\mathcal{H}_{HR}\rangle - \langle\mathcal{H}_{MR}\rangle|} \approx \frac{1/N_{MR}^p - 1/N_{LR}^p}{1/N_{HR}^p - 1/N_{MR}^p} \quad (\text{B2})$$

where  $p$  is the order of convergence [45]. In Figure 8, we show the evolution of the masses of the black holes formed tracked by the apparent horizon finder on base grid resolution, indicating convergence is achieved.

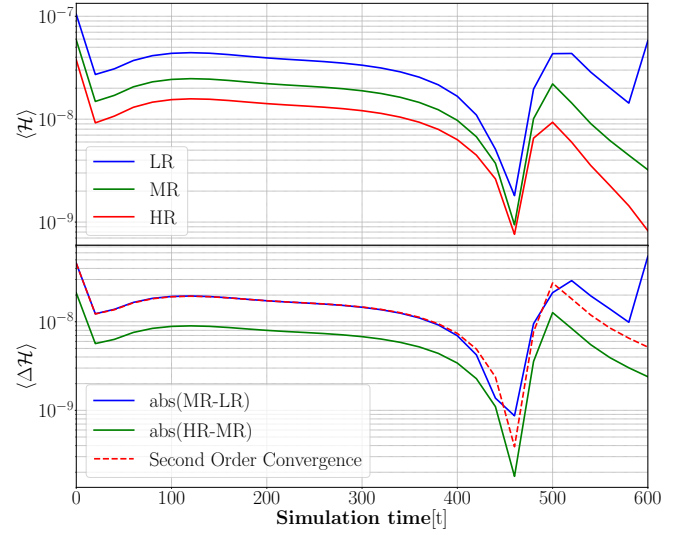


FIG. 7. Hamiltonian convergence tests for volume-average Hamiltonian constraint violation with initial perturbation characteristic wavelength  $\lambda_0 = 20H_0^{-1}$ , and initial non-linearity parameter  $b = 0.0005$ , **Upper Panel**: The volume-averaged Hamiltonian constraint with grid resolutions  $N_{LR} = 128$ ,  $N_{MR} = 144$ ,  $N_{HR} = 160$ , **Lower Panel**: The difference in volume-averaged Hamiltonian constraint between high-middle and middle-low resolutions, and the second order convergence line from abs(HR-MR) to abs(MR-LR) according to Eq. (B2).

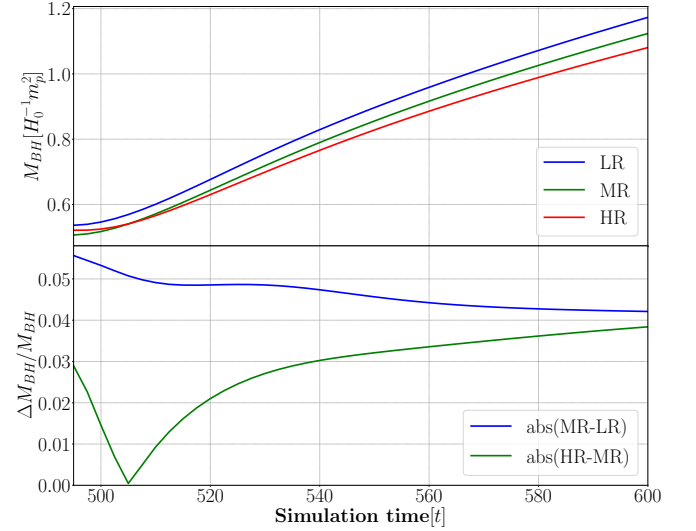


FIG. 8. Convergence tests for black hole mass formed with initial perturbation characteristic wavelength  $\lambda_0 = 20H_0^{-1}$ , and initial non-linearity parameter  $b = 0.0005$ , **Upper Panel**: The measured black hole mass with apparent horizon finder with grid resolutions  $N_{LR} = 128$ ,  $N_{MR} = 144$ ,  $N_{HR} = 160$ , **Lower Panel**: Errors in mass measurements between high-middle and middle-low resolutions showing convergence to  $< 5\%$ .